GIScience & Remote Sensing

ISSN: 1548-1603 (Print) 1943-7226 (Online) Journal homepage: www.tandfonline.com/journals/tgrs20

A singularity regression kriging for spatial prediction

Kai Ren, Yongze Song, Min Chen & Qiang Yu

To cite this article: Kai Ren, Yongze Song, Min Chen & Qiang Yu (2026) A singularity regression kriging for spatial prediction, GIScience & Remote Sensing, 63:1, 2690341, DOI: 10.1080/15481603.2026.2690341

To link to this article: https://doi.org/10.1080/15481603.2026.2690341

Published online: 24 Jul 2026.

GISCIENCE & REMOTE SENSING
2026, VOL. 63, NO. 1, 2690341
https://doi.org/10.1080/15481603.2026.2690341

Taylor & Francis by informa

RESEARCH ARTICLE

OPEN ACCESS Check for updates

A singularity regression kriging for spatial prediction

Kai Ren[a,b,c,d], Yongze Song[d], Min Chen[a,b,c] and Qiang Yu[e]

[a]State Key Laboratory of Climate System Prediction and Risk Management, Nanjing Normal University, Nanjing, People's Republic of China; [b]Key Laboratory of Virtual Geographic Environment (Nanjing Normal University), Ministry of Education, Nanjing, Jiangsu, People's Republic of China; [c]School of Geography, Nanjing Normal University, Nanjing, Jiangsu, People's Republic of China; [d]School of Design and the Built Environment, Curtin University, Perth, Australia; [e]State Key Laboratory of Soil and Water Conservation and Desertification Control, Northwest A&F University, Yangling, Shaanxi, People's Republic of China

ABSTRACT

Accurate spatial prediction remains challenging in heterogeneous environments where environmental variables exhibit nonlinear, multiscale, and non-Gaussian characteristics. Traditional kriging methods rely on simple trend models that cannot adequately capture nonlinear and multiscale spatial structures, leading to degraded prediction performance under complex conditions. This study proposes a singularity regression kriging (SRK) model that explicitly incorporates singularity-based anomaly features derived from environmental covariates into random forest trend estimation, followed by ordinary kriging of the resulting residuals. By computing covariate singularity indices at multiple spatial scales, SRK captures local multiscale heterogeneity without requiring response observations at prediction locations, ensuring robust generalisation under spatial block cross-validation. Simulation experiments demonstrate that SRK consistently improves prediction accuracy relative to ordinary kriging, with particularly significant improvements under skewed and long-tailed distributions. The SRK model is implemented in trace element (Zn and Co) mapping in a mineralised region of Western Australia and evaluated using spatial block cross-validation and parameter sensitivity analysis. Compared with common approaches, including ordinary kriging, regression-based methods, and machine-learning approaches, SRK produces more coherent spatial patterns and reduced prediction uncertainty. These results indicate that explicitly incorporating covariate singularity features into trend estimation enhances both the accuracy and reliability of spatial predictions in heterogeneous environments.

ARTICLE HISTORY
Received 19 January 2026
Accepted 13 June 2026

KEYWORDS
Spatial prediction; kriging; singularity; spatial block cross-validation; geochemical mapping

1. Introduction

Spatial prediction constitutes a central analytical task across diverse scientific domains, including Earth sciences, environmental science, ecology, agricultural resource management, and public health (Austin 2002; Böhner 2005; Böhner and Selige 2006; Jerrett, Gale, and Kontgis 2010; Li 2016; Ren et al. 2025; Sen 2016). The primary objective is to generate reliable inferences of continuous spatial variables at unobserved locations based on a limited set of sampled observations, thereby elucidating the underlying spatial patterns and mechanistic drivers of geophysical or ecological processes (Meyer and Pebesma 2021; Selby and Kockelman 2013). High-quality spatial predictions are essential for ecosystem monitoring, natural resource assessment, environmental risk early-warning systems, and evidence-based decision-making in land-use planning, precision agriculture, air and soil pollution mitigation, exposure assessment in public health, and sustainable urban development (Dadashpoor, Azizi, and Moghadasi 2019; Janssen et al. 2008; Jones and Thornton 2002; Kingsley et al. 2019; Liu, Wu, and Xu 2006; Sparrow et al. 2020; Waller and Gotway 2004; Xu et al. 2025).

Among the range of spatial interpolation techniques, regression kriging (RK) has emerged as one of the most widely adopted geostatistical methods due to its optimal linear unbiased prediction properties under certain assumptions (Hengl, Heuvelink, and Stein 2004; Papritz and Stein 1999). RK operates by

CONTACT Yongze Song yongze.song@curtin.edu.au

decomposing a spatial variable into a deterministic trend component and a stochastic residual component, with the latter modelled through spatial autocorrelation structures captured by variograms (Isaaks and Srivastava 1988; Wu and Li 2013). The efficacy of RK critically hinges on the accurate removal of large-scale trends (detrending) and the assumption that the residuals exhibit stationarity, i.e. their statistical properties remain constant across space (Hengl, Heuvelink, and Rossiter 2007; Holdaway 1996). When these conditions are satisfied, RK can effectively leverage spatial dependence to yield precise predictions at unsampled locations (Odeh, McBratney, and Chittleborough 1995; Papritz and Stein 1999).

Despite their widespread use, traditional kriging methods face significant limitations when faced with complex spatial datasets characterised by nonlinear trends and multiscale heterogeneity (Milne 1991; Vann and Guibal 1998). Conventional detrending approaches, such as linear or polynomial regression, often fall short in adequately capturing intricate nonlinear trends inherent in many environmental and geophysical processes (Beale et al. 2010; Yang et al. 2025). Consequently, the residuals obtained after detrending frequently retain substantial nonlinear and nonstationary structures (Kupfer and Farris 2007). This misalignment can lead to suboptimal prediction performance, as the spatial dependence model may not accurately reflect the true underlying variability (Luo et al. 2026a; Song et al. 2021). While various enhancements to kriging have been proposed, including the integration of machine learning techniques for trend estimation, recent studies have more explicitly advanced geostatistical machine learning for spatial prediction through spatial random forests, random-forest-based spatial interpolation, locally varying geostatistical machine learning, and other hybrid approaches that incorporate spatial dependence or local variation into the predictive framework (Chen et al. 2026; Fouedjio and Arya 2024; Fouedjio and Klump 2019; Liu, Kounadi, and Zurita-Milla 2022; Sekulić et al. 2020; Talebi et al. 2022). More recent studies have also explored alternative strategies for modelling complex and non-stationary spatial dependence, including deep-learning-based approaches and filtering/interpolation methods that relax the conventional stationarity assumption (Bao et al. 2024; Yang et al. 2024). Nevertheless, many existing approaches primarily focus on improving predictive performance by incorporating spatial features or local modelling structures, whereas the potential to improve residual quality within an interpretable regression-kriging approach by explicitly incorporating multiscale anomaly information derived from environmental covariates remains insufficiently explored (Hengl et al. 2018; Li et al. 2019).

This study proposes a singularity regression kriging (SRK) model for spatial prediction by enhancing trend estimation with covariate singularity features. The primary processes of SRK include computing singularity-based anomaly indices from environmental covariates at multiple spatial scales, estimating the spatial trend using a random forest model fitted on the augmented feature matrix of original covariates and their singularity indices, and interpolating the resulting residuals with ordinary kriging to generate final spatial predictions. Unlike conventional geostatistical machine-learning approaches that mainly rely on original covariates or generic spatial features, SRK explicitly incorporates multiscale singularity information derived from environmental covariates into the trend estimation stage. In this study, SRK is implemented for predicting the spatial distributions of Zn and Co in a mining region of Australia, and its performance is evaluated through simulation experiments and a real-data case study.

2. Singularity regression kriging

2.1. Concepts

Regression kriging (RK) decomposes a spatial variable into a deterministic trend component and a stochastic residual component, and relies on stationarity assumptions to model spatial dependence in the residuals (Luo, Wu, and Song 2026b; Odeh, McBratney, and Chittleborough 1995). However, in complex environments, residuals often retain multiscale and nonlinear spatial structures that are insufficiently captured by conventional detrending approaches, leading to degraded kriging performance. To address this limitation, we introduce a singularity regression kriging (SRK) model that incorporates singularity-based anomaly indices derived from environmental covariates into the random forest feature set for trend estimation. For each covariate, a singularity index is computed by measuring local multiscale contrast across a range of spatial scales. These singularity indices capture spatial heterogeneity and anomalous behaviour that is not readily represented by the original covariate values alone. By augmenting the covariate set with corresponding singularity features, the random forest trend estimator is better equipped to explain spatially structured variation, resulting in residuals that are closer to stationary and therefore more amenable to ordinary kriging interpolation.

2.2. SRK model

The SRK model is designed for spatial prediction by integrating covariate singularity feature construction, nonlinear trend estimation via random forest, and geostatistical interpolation of residuals. Traditional kriging approaches, particularly ordinary kriging (OK), assume a constant mean and therefore cannot explicitly represent complex spatial trends (Cressie 1988; Oliver and Webster 1990), while RK typically relies on linear trend models and may leave nonlinear structures in the residuals (Hengl, Heuvelink, and Rossiter 2007; Hengl, Heuvelink, and Stein 2004). SRK addresses these limitations by enhancing trend estimation with multiscale singularity features so that the remaining residuals become closer to stationary and more suitable for ordinary kriging, ultimately improving spatial prediction accuracy.

Let D denote the study domain, and let $\mathbf{s}_i \in D$, $i = 1,\ldots,n$, denote sampled locations, with $\mathbf{s}_0 \in D$ denoting an unsampled prediction location. The target variable observed at $\mathbf{s}_i$ is denoted by $Z(\mathbf{s}_i)$. The original predictor variables are denoted by $X_k(\mathbf{s})$, $k = 1,\ldots,p$, where p is the number of predictors and n is the number of observed samples. In this study, the predictor variables are assumed to be available across the prediction domain so that singularity features and trend estimates can be evaluated at unsampled locations.

2.2.1. Singularity feature construction

The first step constructs singularity-based anomaly indices from environmental covariates. For each covariate X_k, $k = 1,\ldots,p$, the singularity index $\alpha_k(\mathbf{s})$ is defined through the local scaling behaviour of the covariate measure within neighbourhoods of increasing size (Cheng 2012, 2017, 2018). In a two-dimensional spatial domain, the theoretical singularity relationship can be written as:

$$C_k(A(\mathbf{s}, r)) \propto r^{\alpha_k(\mathbf{s})-2}, \tag{1}$$

where $C_k(A(\mathbf{s}, r))$ denotes the local covariate intensity of X_k within the neighbourhood $A(\mathbf{s}, r)$, r is the spatial scale, and 2 is the Euclidean dimension of the spatial domain. The singularity index $\alpha_k(\mathbf{s})$ therefore characterises how the local covariate intensity changes with scale around location $\mathbf{s}$. In this study, $C_k(A(\mathbf{s}, r))$ is estimated by the mean absolute covariate value within the square window $A(\mathbf{s}, r)$ centred at $\mathbf{s}$:

$$C_k(A(\mathbf{s}, r)) = \frac{1}{|A(\mathbf{s}, r)|} \sum_{\mathbf{s}' \in A(\mathbf{s}, r)} |X_k(\mathbf{s}')|, \tag{2}$$

where $\mathbf{s}'$ denotes a reference point within the window and $|A(\mathbf{s}, r)|$ denotes the number of such reference points.

Repeating this computation across a set of scales $r_1 < r_2 < \cdots < r_J$ yields a log-log linear model:

$$\log C_k(A(\mathbf{s}, r)) = (\alpha_k(\mathbf{s}) - 2)\log r + c_k(\mathbf{s}) + e_{k,r}, \tag{3}$$

where $c_k(\mathbf{s})$ is a local intercept term and $e_{k,r}$ is a scale-specific residual term. The singularity index is estimated as the fitted slope of this log-log regression plus two:

$$\alpha_k(\mathbf{s}) = \hat{\beta}_{1,k}(\mathbf{s}) + 2, \tag{4}$$

where $\hat{\beta}_{1,k}(\mathbf{s})$ is the ordinary least-squares slope of $\log C_k(A(\mathbf{s}, r))$ on $\log r$ across the selected spatial scales. The value $\alpha_k(\mathbf{s}) = 2$ corresponds to a spatially uniform field and serves as a neutral reference; $\alpha_k(\mathbf{s}) < 2$ indicates local enrichment (positive anomaly), and $\alpha_k(\mathbf{s}) > 2$ indicates local depletion. Locations where an insufficient number of valid scales are available are assigned the neutral value of 2.

As singularity indices are computed from covariates rather than from response observations, they can be evaluated at any spatial location, including unsampled prediction locations. This property ensures that the anomaly features remain well-defined under spatial cross-validation schemes that withhold geographically contiguous test blocks. To avoid near-constant singularity features that add noise rather than signal, features with training-set standard deviation below a minimum threshold are excluded from the augmented feature set.

2.2.2. Trend estimation

The second step fits a random forest model using the original covariates augmented with the singularity features retained after the standard-deviation filter. Let $q \le p$ denote the number of retained singularity features, indexed over the selected subset of covariates after variance filtering. The augmented feature set at location $\mathbf{s}_i$ is:

$$\mathcal{F}(\mathbf{s}_i) = \{X_1(\mathbf{s}_i), \ldots, X_p(\mathbf{s}_i),\ \alpha_{k_1}(\mathbf{s}_i), \ldots, \alpha_{k_q}(\mathbf{s}_i)\}, \tag{5}$$

where $k_1, \ldots, k_q \subseteq \{1, \ldots, p\}$ are the indices of the covariates whose singularity features passed the variance filter.

A random forest model (Breiman 2001) is trained on the augmented feature set to estimate the spatial trend:

$$\hat{\mu}(\mathbf{s}_i) = g(\mathcal{F}(\mathbf{s}_i)), \tag{6}$$

where $g(\cdot)$ denotes the fitted random forest model. The corresponding residuals are:

$$\varepsilon(\mathbf{s}_i) = Z(\mathbf{s}_i) - \hat{\mu}(\mathbf{s}_i). \tag{7}$$

As the singularity-augmented random forest absorbs both the covariate-driven trend and the multiscale anomaly structure, the residuals $\varepsilon(\mathbf{s}_i)$ are expected to be closer to spatial stationarity than residuals obtained from a conventional random forest fitted on the original covariates alone.

2.2.3. Residual kriging and prediction

The third step applies ordinary kriging to the sampled residuals $\varepsilon(\mathbf{s}_i)$. A variogram model is first fitted to characterise the spatial covariance structure of the residuals. The ordinary kriging predictor at an unsampled location $\mathbf{s}_0$ is then:

$$\hat{\varepsilon}(\mathbf{s}_0) = \sum_{i=1}^{n} \lambda_i\, \varepsilon(\mathbf{s}_i), \tag{8}$$

where the weights λ_i are obtained by solving the ordinary kriging system subject to the unbiasedness constraint $\sum_{i=1}^{n} \lambda_i = 1$. The final SRK prediction at location $\mathbf{s}_0$ is:

$$\hat{Z}(\mathbf{s}_0) = \hat{\mu}(\mathbf{s}_0) + \hat{\varepsilon}(\mathbf{s}_0), \tag{9}$$

where $\hat{\mu}(\mathbf{s}_0) = g(\mathcal{F}(\mathbf{s}_0))$ is the singularity-augmented random forest trend evaluated at the prediction location. The prediction uncertainty is quantified by the kriging standard error:

$$\delta(\mathbf{s}_0) = \sqrt{\sigma_K^2(\mathbf{s}_0)}, \tag{10}$$

where $\sigma_K^2(\mathbf{s}_0)$ is the kriging variance obtained directly from the ordinary kriging system.

2.3. Simulation data analysis

2.3.1. Simulation design

As an initial evaluation, the predictive performance of the proposed SRK model was assessed under controlled conditions using simulated data generated on a regular 20×20 grid. A spatially autocorrelated base field was first simulated using a spherical variogram model, and an auxiliary covariate field was then constructed to maintain a strong but imperfect spatial association with the response field. Based on these two base fields, three simulation scenarios were designed to represent increasing levels of distributional complexity. These experiments were intended as controlled illustrative tests for examining the robustness of SRK under different distributional conditions, rather than for reproducing a fully realistic large-scale geological system. The exact implementation details, including the simulated data-generation code, model computation workflow, and plotting scripts, are provided in the public code repository accompanying this study.

The first scenario retained the shifted base fields and therefore approximated a normal spatial distribution, serving as a baseline case that is broadly consistent with the assumptions of conventional kriging. The second scenario applied a nonlinear transformation to generate a positively skewed distribution, while the third scenario applied a stronger nonlinear transformation to produce a long-tailed distribution with more extreme heterogeneity. Figure 1 shows the spatial patterns and corresponding histograms of these three simulated datasets, with panels (a), (b), and (c) representing the normal, skewed, and long-tailed cases, respectively. Together, these scenarios provide a systematic basis for evaluating the performance of SRK across spatial fields with progressively stronger non-Gaussianity and nonlinearity.

To evaluate the predictive performance of the SRK model, three standard statistical metrics were employed for the validation data: the coefficient of determination (R^2), the root mean square error (RMSE), and the mean absolute error (MAE). These metrics are calculated as follows:

$$R^2 = 1 - \frac{\sum_{i=1}^{n} (y_i - \hat{y}_i)^2}{\sum_{i=1}^{n} (y_i - \bar{y})^2} \tag{11}$$

$$RMSE = \sqrt{\frac{1}{n} \sum_{i=1}^{n} (\hat{y}_i - y_i)^2} \tag{12}$$

$$MAE = \frac{1}{n} \sum_{i=1}^{n} |\hat{y}_i - y_i| \tag{13}$$

where y_i denotes the observed value in the validation data, $\hat{y}_i$ indicates the corresponding predicted value, $\bar{y}$ is the mean of the observed validation values, and n represents the number of validation observations.

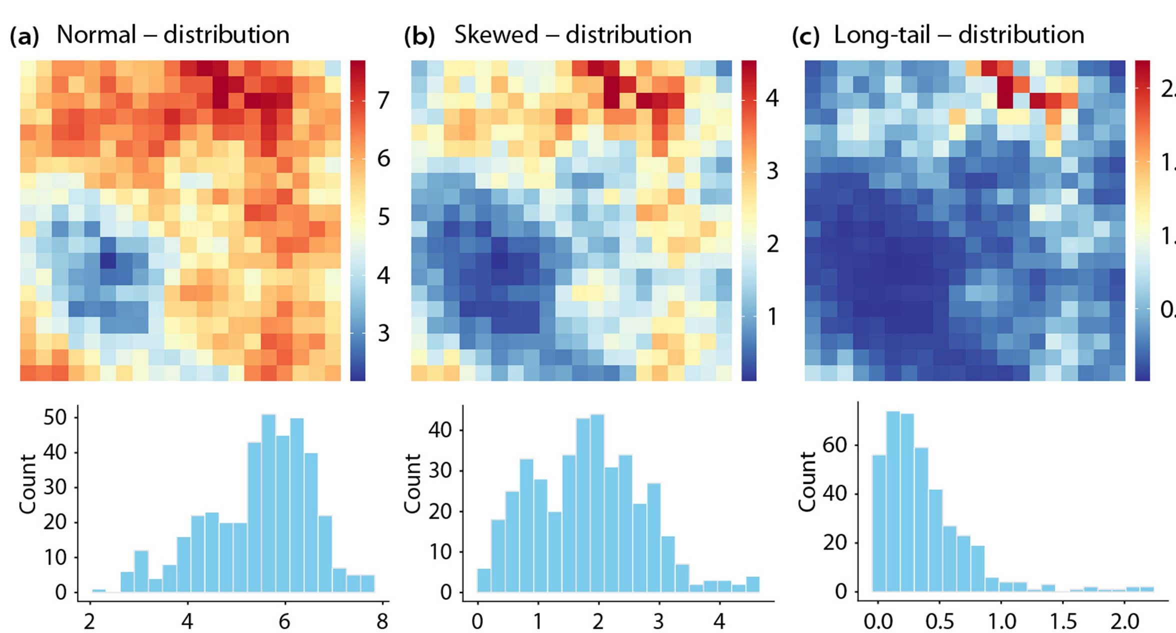

Figure 1. Spatial distributions and histograms of the three simulated datasets: (a) normal, (b) skewed, and (c) long-tailed.

2.3.2. Simulation results

Figure 2 illustrates the SRK modelling process across the three simulation scenarios. The covariate singularity maps reveal clear spatial heterogeneity that aligns with the distributional structure of the simulated response variable, indicating that singularity indices computed from covariates effectively capture local anomalous behaviour. The scatter plots in Figure 2(b), (f), and (j) show that singularity features exhibit structured relationships with the response variable, confirming their informative value as augmented predictors. Variable importance charts in Figure 2(c), (g), and (k) indicate that the singularity features contribute substantially to random forest predictions, with their relative importance increasing under skewed and long-tailed distributions. The cross-validation scatter plots in Figure 2(d), (h), and (l) demonstrate that SRK predictions are generally closer to the 1:1 line than ordinary kriging, with visibly reduced dispersion, and the improvement becomes more evident as the distribution departs further from normality.

Table 1 summarises the predictive performance of SRK relative to OK across the three simulated datasets. Across all scenarios, SRK consistently outperforms OK. For the normal, skewed, and long-tailed datasets, SRK increases R^2 by 0.096 (11.0%), 0.133 (16.0%), and 0.204 (27.8%), respectively, while reducing RMSE by 0.189 (52.4%), 0.199 (55.0%), and 0.093 (52.5%). Similar improvements are also observed for MAE. The magnitude of improvement generally increases as the distribution departs further from Gaussian assumptions, indicating that SRK is particularly effective under skewed and long-tailed conditions, where the singularity-augmented random forest trend estimator is better able to capture complex spatial structures than ordinary kriging.

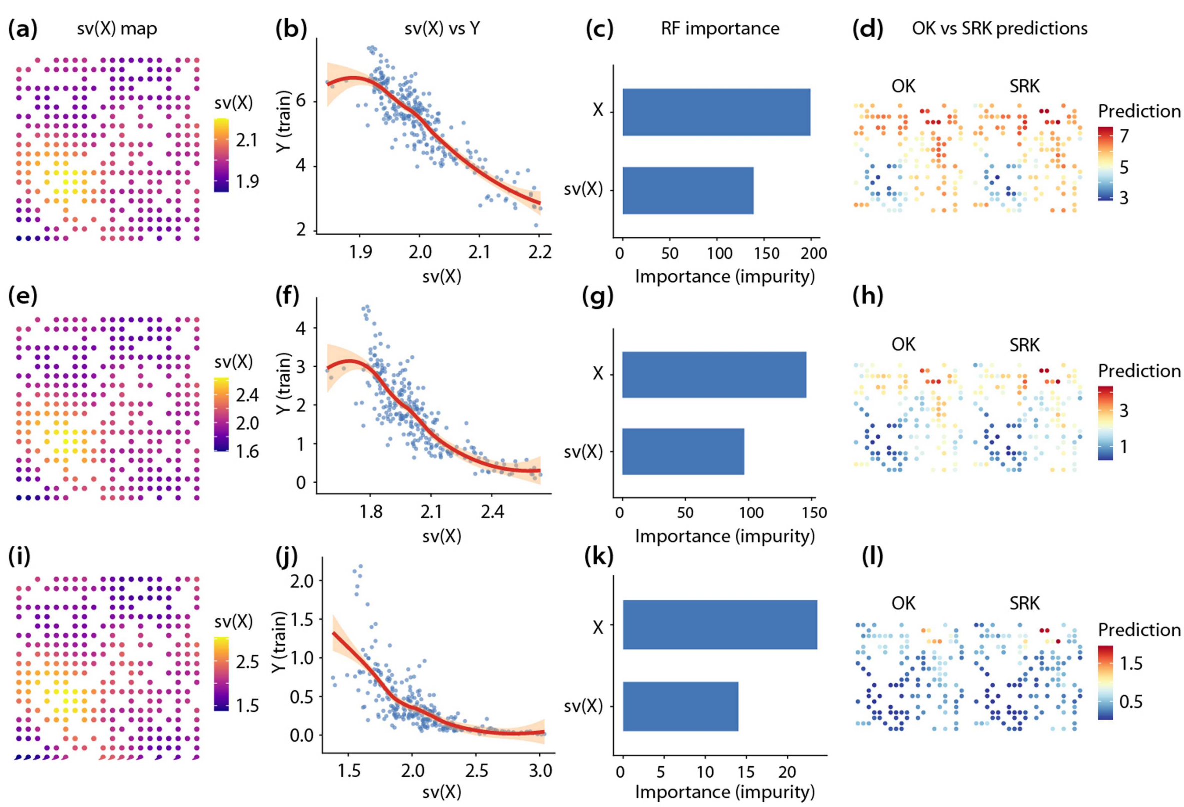

Figure 2. Illustration of the SRK modelling process using three simulated datasets, including the normal (a–d), skewed (e–h), and long-tailed (i–l) cases, showing the spatial distribution of the covariate singularity index (a, e, i), the relationship between the singularity index and the response variable for training samples (b, f, j), the random forest variable importance comparing original covariate and singularity features (c, g, k), and comparisons between SRK and ordinary kriging predictions (d, h, l).

Table 1. Performance comparison between ordinary kriging (OK) and singularity regression kriging (SRK) across simulated spatial datasets.

	R^2			RMSE			MAE		
Simulation spatial data	OK	SRK	Δ (abs, %)	OK	SRK	Δ (abs, %)	OK	SRK	Δ (abs, %)
Dataset 1: Normal distribution	0.876	0.972	+0.096 (↑ 11.0%)	0.361	0.172	−0.189 (↓ 52.4%)	0.284	0.137	−0.147 (↓ 51.5%)
Dataset 2: Skewed distribution	0.833	0.966	+0.133 (↑ 16.0%)	0.361	0.162	−0.199 (↓ 55.0%)	0.265	0.120	−0.145 (↓ 54.8%)
Dataset 3: Long-tail distribution	0.736	0.940	+0.204 (↑ 27.8%)	0.178	0.085	−0.093 (↓ 52.5%)	0.107	0.056	−0.051 (↓ 48.0%)

Note: Δ reports the absolute difference first and the relative percentage change in parentheses for SRK relative to OK.

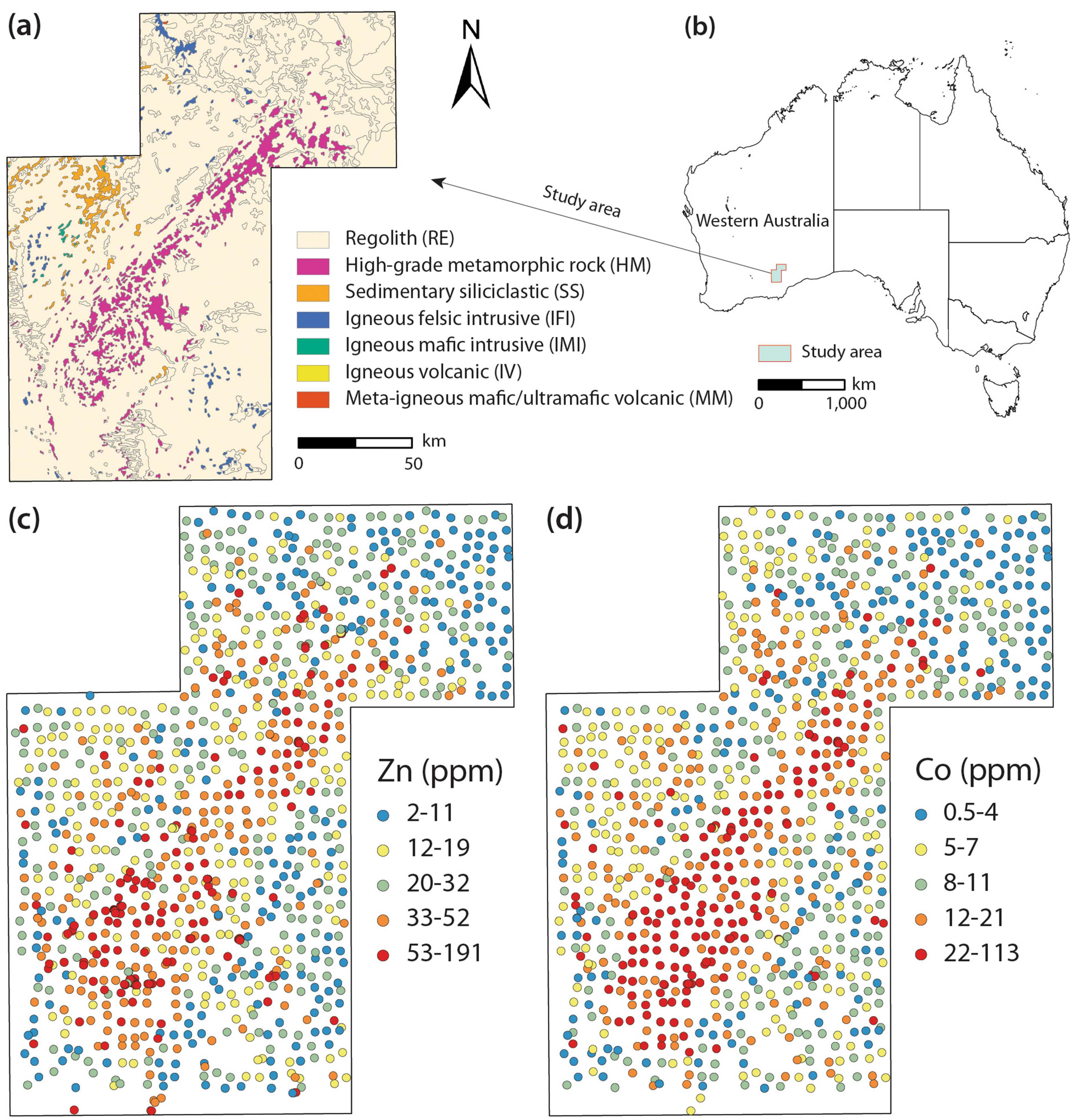

Figure 3. Study area in Western Australia (b), lithological distribution (a), and spatial distributions of Zn (c) and Co (d) samples within the study area.

3. Application: spatial prediction of trace elements

3.1. Study area and data

In this study, the SRK model is implemented to predict the spatial distributions of trace elements (Zn and Co) in a mining region of Western Australia characterised by pronounced lithological heterogeneity (Figure 3(b)). Geochemical data for two trace elements, Zn (n = 1105) and Co (n = 998), were obtained from the GSWA Geochemistry database (DMIRS-047) (Department of Energy et al. 2019). The spatial distributions of these samples (Figure 3(c) and (d)) exhibit clear clustering patterns, indicating strong geological controls on trace element enrichment.

To represent the key environmental factors governing trace element variability, a set of lithological and topographic covariates was assembled for spatial modelling. Lithological information was sourced from Geoscience Australia and represents the dominant parent material across the study area (Geoscience Australia 2012), as illustrated in Figure 3(a). In addition, topographic variables including elevation, slope, and aspect were derived from a Digital Elevation Model (DEM) (Geoscience Australia 2015) to capture terrain-related redistribution processes. Structural features such as faults were not considered, as no mapped fault systems occur within the defined study extent (Raymond et al. 2012).

3.2. Experiment design

The experimental workflow for predicting trace element concentrations was structured into three distinct phases: data preprocessing and variable selection, singularity-augmented trend modelling and residual kriging, and comprehensive model validation. The overall methodological workflow is illustrated in Figure 4.

3.2.1. Data preprocessing and variable selection

The initial phase focused on standardising the input datasets and selecting optimal covariates. While topographic variables (e.g. elevation, slope) are naturally continuous, lithological data are categorical vector polygons. To quantify the spatial influence of lithology on geochemical dispersion and incorporate it into the regression models, we constructed a continuous proximity variable for each target lithological unit using a truncated linear decay function (Luo, Wu, and Song 2026b; Song 2023):

$$x(\mathbf{s}) = \begin{cases} 1, & \mathbf{s} \in L, \\ 1 - \frac{d(\mathbf{s}, L)}{10\text{km}}, & \mathbf{s} \notin L \text{ and } 0 < d(\mathbf{s}, L) \leq 10 \text{ km}, \\ 0, & \mathbf{s} \notin L \text{ and } d(\mathbf{s}, L) > 10 \text{ km}, \end{cases} \tag{14}$$

where L denotes the target lithological unit, $\mathbf{s}$ is the target location, and $d(\mathbf{s}, L)$ is the shortest Euclidean distance from $\mathbf{s}$ to the boundary of L when $\mathbf{s}$ lies outside the lithological unit. Thus, the proximity variable is defined as 1 for locations inside the target lithological unit, decreases linearly to 0 within a 10 km external buffer, and is set to 0 beyond this distance (Song 2022, 2023).

Following this transformation, a Spearman correlation analysis was conducted to examine the relationships between trace elements and the candidate covariates. Only variables showing statistically significant correlations ($p < 0.05$) were retained for the subsequent modelling phase.

3.2.2. Singularity feature engineering and trend modelling

In the second phase, the SRK model was used to predict the spatial distributions of Zn and Co by integrating covariate singularity feature construction, random forest trend estimation, and residual kriging. For each predictor variable, singularity indices were computed from multiscale neighbourhoods of the covariate field following the formulation of (Cheng 2017). In this study, the singularity analysis was conducted over spatial scales ranging from 2 to 20 km at 2-km intervals. To ensure numerical stability, each scale was required to include at least three valid neighbouring samples, and at least two valid scales were required for singularity estimation. The resulting singularity indices were treated as covariate anomaly features and combined with the original predictors to form an augmented feature set. To avoid introducing near-constant singularity variables, only singularity features with a standard deviation greater than 0.5 were

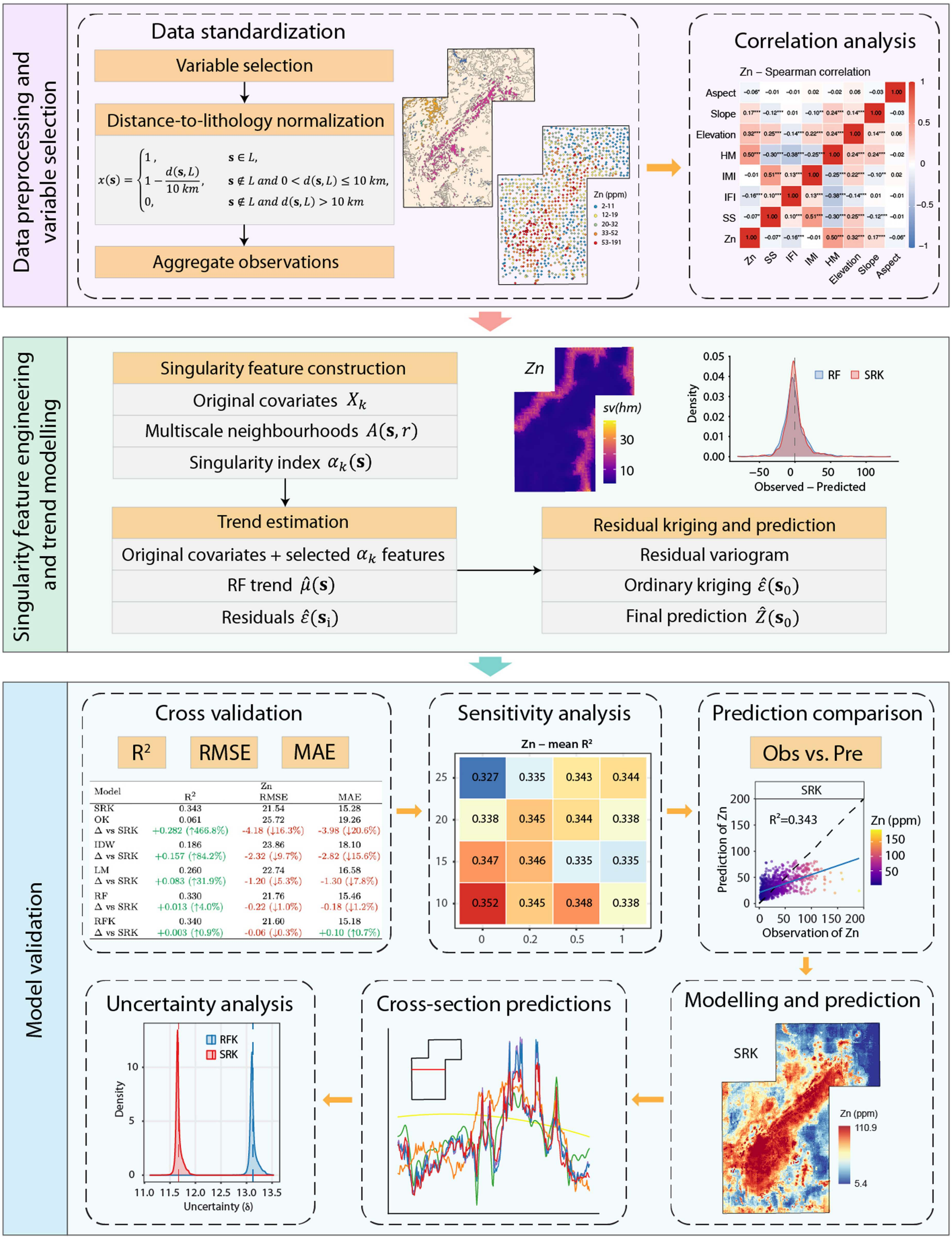

Figure 4. Workflow of the singularity regression kriging (SRK) model for trace element prediction in a mining region.

retained. A random forest model with 500 trees was then fitted on the augmented feature set to estimate the spatial trend, and the resulting residuals were subsequently interpolated using ordinary kriging to generate the final spatial predictions. For the ordinary kriging step, variogram fitting was implemented using the autoKrige function in the R package automap, which automatically selects the variogram from standard candidate model families provided by the package rather than specifying a single model a priori. Anisotropy was not explicitly tested or fitted, and the kriging interpolation was therefore performed under an isotropic assumption.

3.2.3. Model validation

In the final stage, model performance was evaluated through spatial block cross-validation (5-fold, 15 km block size) using multiple accuracy metrics, including the coefficient of determination, root mean squared error, and mean absolute error. The predictive performance of the proposed SRK model was systematically compared with five benchmark methods, namely ordinary kriging (OK), inverse distance weighting (IDW), linear regression (LM), random forest (RF), and random forest kriging (RFK). Comparative analyses were conducted in terms of prediction accuracy, spatial prediction patterns, and associated uncertainty. In addition, a parameter sensitivity analysis was performed by varying the maximum singularity scale and the singularity feature selection threshold to examine the robustness of the SRK model under different parameter settings. Additional evaluations, including uncertainty analysis and cross-section comparisons, were further employed to assess the robustness and practical applicability of the proposed model under complex spatial conditions.

4. Results

4.1. Data preprocessing and variable selection

Lithological variables were first screened based on the spatial distribution of lithological units and the distances between sample locations and lithological boundaries. Seven lithological types were initially considered (SS, HM, IFI, IMI, IV, MM, and RE; Figure 3(a)). RE occupies the majority of the study area, resulting in most samples being located within this unit and providing limited discriminatory information for spatial prediction; therefore, RE was excluded. IV and MM cover only very small areas and are sparsely distributed, suggesting a negligible influence on trace-element variability at the regional scale. Consequently, four lithological variables (SS, HM, IFI, and IMI) were retained for subsequent analyses.

For the selected lithological variables, distances from sample points to lithological surfaces were calculated and transformed using a linear truncation scheme, where values equal to 1 were assigned within lithological units, linearly decreasing to 0 with increasing distance up to 10 km, and set to 0 beyond this threshold. This transformation reflects the assumption that lithological influence on trace-element concentrations diminishes with distance and becomes negligible beyond 10 km. The same procedure was applied to prediction grids with a spatial resolution of 500 m. Terrain variables (slope, aspect, and elevation) were extracted directly from DEM-derived raster values at both sample and grid locations. For trace-element data (Zn and Co), multiple measurements at identical locations were averaged to ensure a single representative value per sample point.

4.2. Spearman correlation

Spearman correlation analysis was employed to examine the monotonic relationships between trace element concentrations and explanatory variables, including lithological and terrain factors (Figure 5). The results revealed distinct controlling factors for each element. Zn showed statistically significant associations ($p < 0.05$) with multiple predictors, including SS, IFI, and HM lithologies, as well as terrain variables (slope, aspect, and elevation). In contrast, Co was primarily associated with IFI, HM, and Elevation. Based on these statistically significant relationships, element-specific subsets of predictors were selected to reduce redundancy and enhance the explanatory power of subsequent spatial modelling.

4.3. Singularity feature engineering and residual analysis

The SRK model augments the predictor set with covariate singularity indices computed at multiple spatial scales, enabling the random forest trend estimator to capture local multiscale heterogeneity that is not represented by the original covariate values alone. Figure 6 presents the covariate singularity maps, random

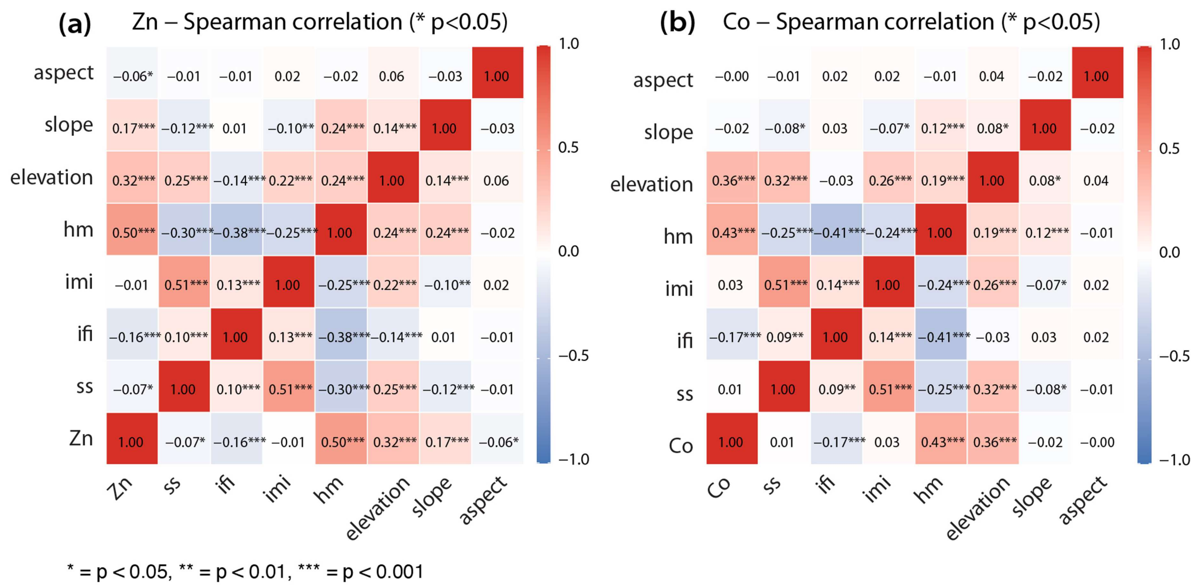

Figure 5. Spearman correlation matrices between trace elements and explanatory variables for (a) Zn and (b) Co.

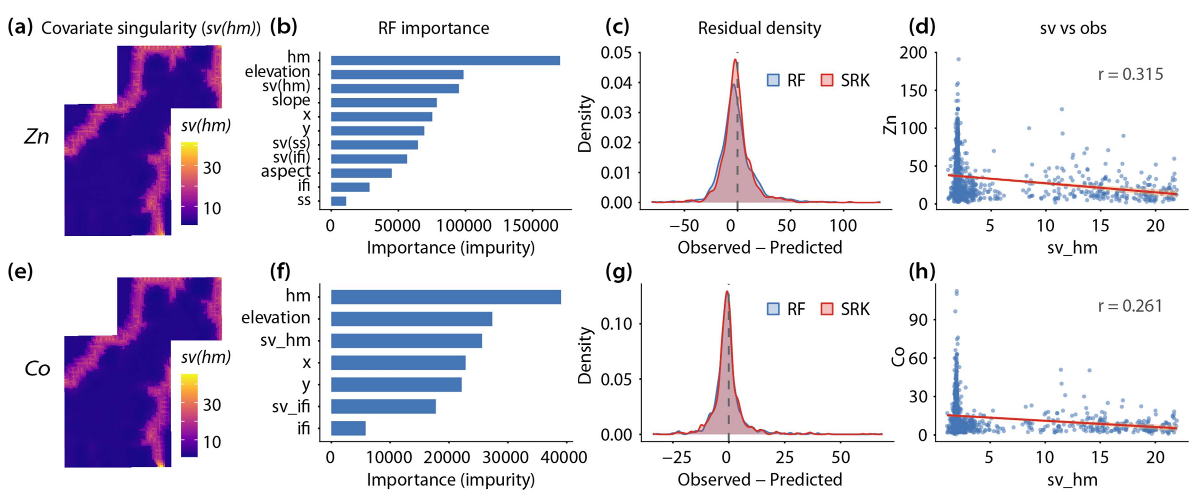

Figure 6. Analysis of covariate singularity features and residual improvement in the SRK model for Zn (a–d) and Co (e–h). (a, e) Spatial distributions of the selected covariate singularity feature, *sv(hm)*. (b, f) Random forest variable importance, showing the relative contribution of original covariates and singularity features. (c, g) Residual density distributions for RF and SRK, illustrating the effect of singularity feature augmentation on residual concentration and spread. (d, h) Relationships between the singularity feature *sv_hm* and the observed element concentration, with the fitted trend line and correlation coefficient shown.

forest variable importance, residual density comparisons, and relationships between singularity features and observed concentrations for Zn and Co. The singularity maps in Figure 6(a) and (e) reveal clear spatial heterogeneity, with elevated singularity values concentrated along lithological transition zones and mineralised belts, indicating that the singularity features capture spatially structured local anomalies beyond the information contained in the original covariates.

The variable importance charts in Figure 6(b) and (f) show that singularity features contribute substantially to the random forest trend estimation for both Zn and Co, with *sv(hm)* ranking among the most important predictors. At the same time, the residual density plots in Figure 6(c) and (g) indicate that SRK residuals are more concentrated around zero than those from the standard random forest model, suggesting reduced residual spread and improved suitability for subsequent ordinary kriging. The scatter plots in Figure 6(d) and (h) further confirm that the selected singularity feature is associated with observed Zn and Co concentrations, supporting its value as an informative augmented predictor in the SRK model.

4.4. Model validation

Spatial block cross-validation (5-fold, 15 km block size) was performed to evaluate the predictive accuracy of the SRK model against five benchmark models (OK, IDW, LM, RF, and RFK). Table 2 summarises the cross-validation metrics, where the rows "Δ vs SRK" report both the absolute differences and the relative percentage changes. For Zn, SRK achieved the best overall performance ($R^2 = 0.343$, RMSE = 21.54, MAE = 15.28), improving upon RFK by 0.003 in R^2 (0.9%) and reducing RMSE by 0.06 (0.3%), although MAE was slightly higher by 0.10 (0.7%). Relative to OK, SRK improved R^2 by 0.282 (466.8%), reduced RMSE by 4.18 (16.3%), and reduced MAE by 3.98 (20.6%). For Co, SRK also ranked first ($R^2 = 0.353$, RMSE = 10.45, MAE = 6.47), increasing R^2 by 0.008 (2.3%) and reducing RMSE by 0.03 (0.3%) relative to RFK, while MAE was slightly higher by 0.06 (0.9%). Compared with OK, SRK improved R^2 by 0.205 (138.5%), reduced RMSE by 1.59 (13.2%), and reduced MAE by 1.56 (19.4%). Overall, these results indicate that SRK critically improves upon the conventional geostatistical benchmarks and provides modest but stable improvements over the covariate-based RF and RFK benchmarks under spatial block cross-validation.

Following cross-validation, a parameter sensitivity analysis was conducted to examine the robustness of the SRK model to different combinations of maximum singularity scale and singularity feature selection threshold (Figure 7). The heatmaps in Figure 7 show that model performance remains relatively stable across a wide range of parameter settings for both Zn and Co, with only modest variation in mean R^2 and RMSE. For Zn, the highest mean R^2 was obtained at a maximum scale of 10 km. A comparable pattern was observed for Co, where the best-performing parameter combination also differed only slightly from the baseline. The relative-change analysis in Figure 7(e) further indicates that most parameter combinations result in changes within approximately ± 5% of the baseline for both R^2 and RMSE, confirming that SRK is not overly sensitive to moderate parameter perturbations. These results suggest that the proposed SRK model is robust and that the selected baseline parameter setting provides a reasonable balance between predictive accuracy and model stability.

The observed–predicted scatter plots in Figure 8 illustrate the predictive relationships for Zn and Co obtained from SRK and the five benchmark models. Overall, the point clouds of SRK are more closely aligned with the 1:1 line than those of OK, IDW, and LM, indicating better agreement between predictions and observations. This pattern is also reflected in the R^2 values shown in the panels. For Zn, SRK achieves the highest R^2 (0.343), slightly exceeding RFK (0.340) and RF (0.330), while for Co, SRK again ranks first with an R^2 of 0.353, compared with 0.345 for RFK and 0.342 for RF. In contrast, OK shows the lowest R^2 values for both Zn and Co, suggesting the weakest predictive consistency. These scatter plots suggest that SRK provides slightly stronger observed–predicted agreement than the other compared models, although the difference relative to RF and RFK is modest.

Spatial prediction maps for Zn and Co derived from SRK and the five benchmark models are shown in Figure 9. Overall, the SRK maps show clearer spatial structure and more coherent enrichment patterns than

Table 2. Performance comparison of six spatial prediction models for Zn and Co. Values of R^2, RMSE, and MAE are based on 5-fold spatial block cross-validation with a block size of 15 km. For each benchmark model, the row "Δ vs SRK" reports the absolute difference followed by the relative percentage change in parentheses.

	Zn			Co		
Model	R^2	RMSE	MAE	R^2	RMSE	MAE
SRK	0.343	21.54	15.28	0.353	10.45	6.47
OK	0.061	25.72	19.26	0.148	12.04	8.03
Δ vs SRK	+0.282 (↑ 466.8%)	−4.18 (↓ 16.3%)	−3.98 (↓ 20.6%)	+0.205 (↑ 138.5%)	−1.59 (↓ 13.2%)	−1.56 (↓ 19.4%)
IDW	0.186	23.86	18.10	0.266	11.15	7.42
Δ vs SRK	+0.157 (↑ 84.2%)	−2.32 (↓ 9.7%)	−2.82 (↓ 15.6%)	+0.087 (↑ 32.7%)	−0.70 (↓ 6.3%)	−0.95 (↓ 12.8%)
LM	0.260	22.74	16.58	0.237	11.33	7.48
Δ vs SRK	+0.083 (↑ 31.9%)	−1.20 (↓ 5.3%)	−1.30 (↓ 7.8%)	+0.116 (↑ 48.9%)	−0.88 (↓ 7.8%)	−1.01 (↓ 13.5%)
RF	0.330	21.76	15.46	0.342	10.50	6.46
Δ vs SRK	+0.013 (↑ 4.0%)	−0.22 (↓ 1.0%)	−0.18 (↓ 1.2%)	+0.011 (↑ 3.2%)	−0.05 (↓ 0.5%)	+0.01 (↑ 0.1%)
RFK	0.340	21.60	15.18	0.345	10.48	6.41
Δ vs SRK	+0.003 (↑ 0.9%)	−0.06 (↓ 0.3%)	+0.10 (↑ 0.7%)	+0.008 (↑ 2.3%)	−0.03 (↓ 0.3%)	+0.06 (↑ 0.9%)

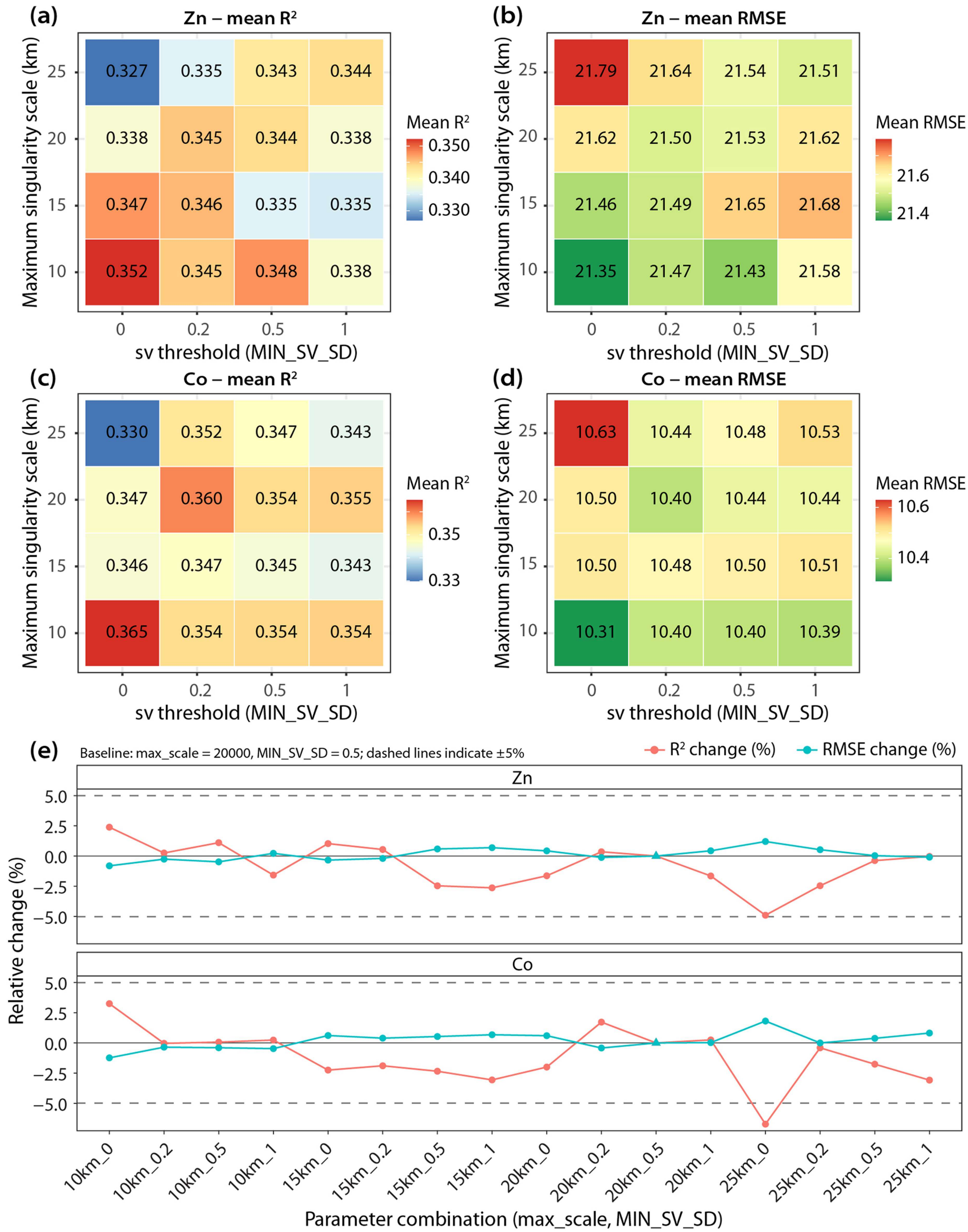

Figure 7. Sensitivity analysis of the SRK model under different parameter combinations for Zn and Co. (a, c) Heatmaps of mean R^2 for Zn and Co, respectively, across combinations of maximum singularity scale and singularity feature selection threshold. (b, d) Heatmaps of mean RMSE for Zn and Co, respectively, under the same parameter settings. (e) Relative changes in R^2 and RMSE with respect to the baseline parameter settings with the maximum singularity scale of 20 km and singularity selection threshold of 0.5 for Zn and Co, with dashed lines indicating the ± 5% range used to assess model robustness.

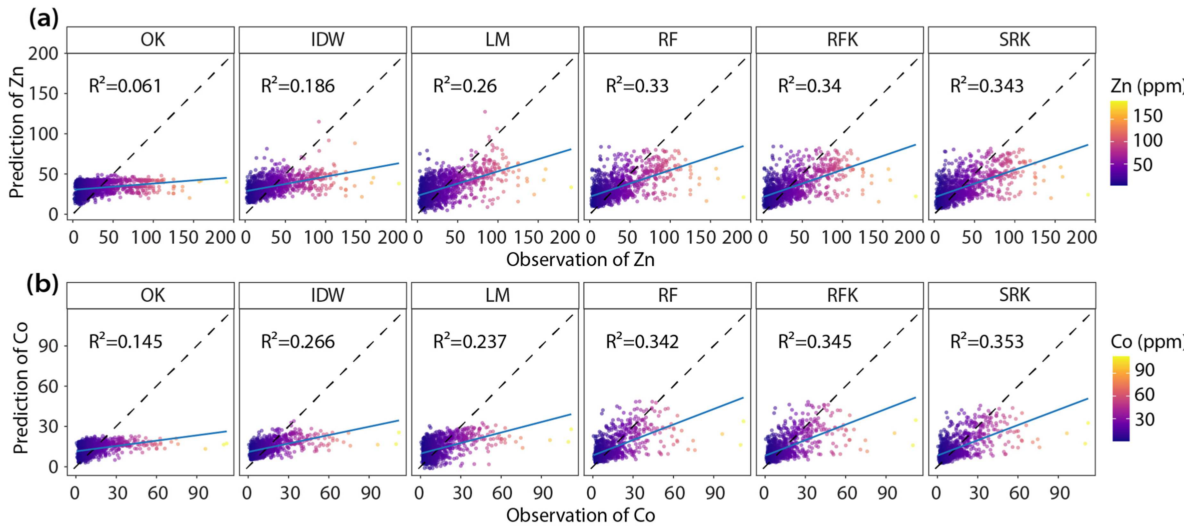

Figure 8. Comparisons between observations and predictions of Zn and Co concentrations for the validation data under spatial block cross-validation of the SRK and benchmark models (OK, IDW, LM, RF, and RFK).

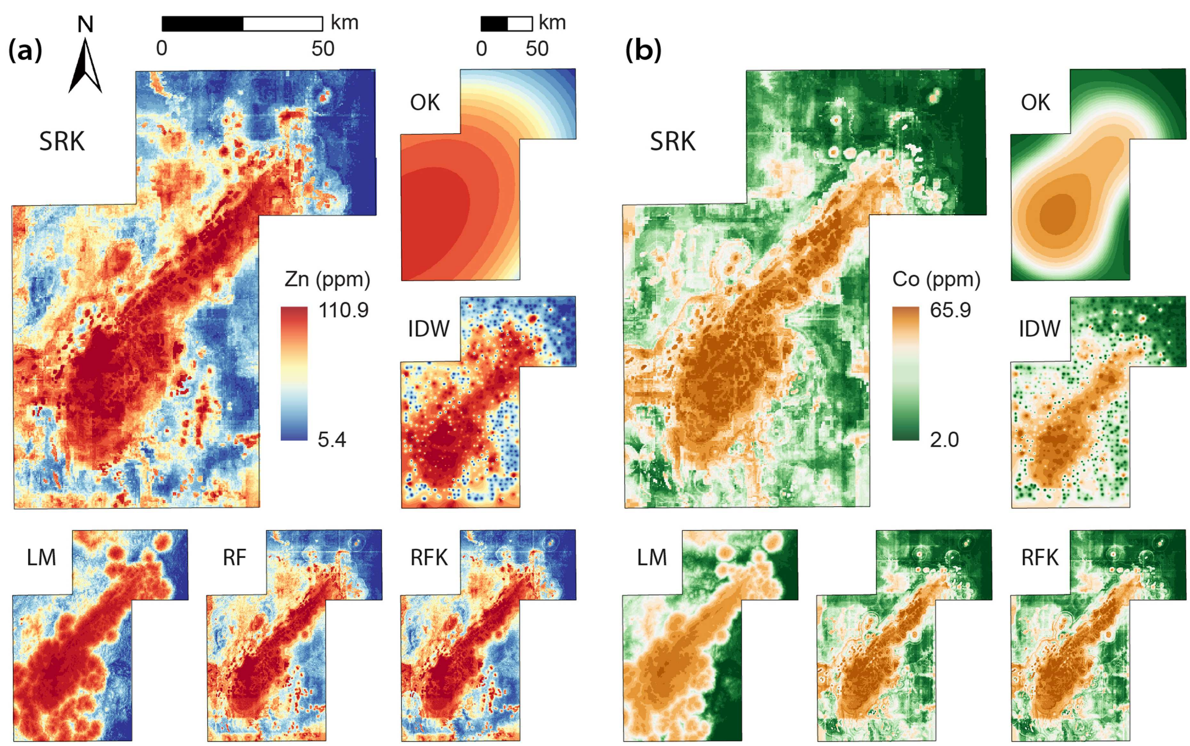

Figure 9. Spatial predictions of trace elements, Zn (a) and Co (b), in the study area using the SRK model and benchmark methods (OK, IDW, LM, RF, and RFK). For each element, the six prediction maps are displayed using a unified colour scale to ensure direct visual comparability across models.

the conventional geostatistical methods. OK and LM produce overly smooth surfaces, whereas IDW generates fragmented local artefacts around sample locations. RF and RFK recover more spatial detail, but the SRK predictions appear more balanced in preserving both regional continuity and local heterogeneity. These visual patterns suggest that incorporating covariate singularity features helps SRK better reproduce realistic spatial variation in trace-element distributions.

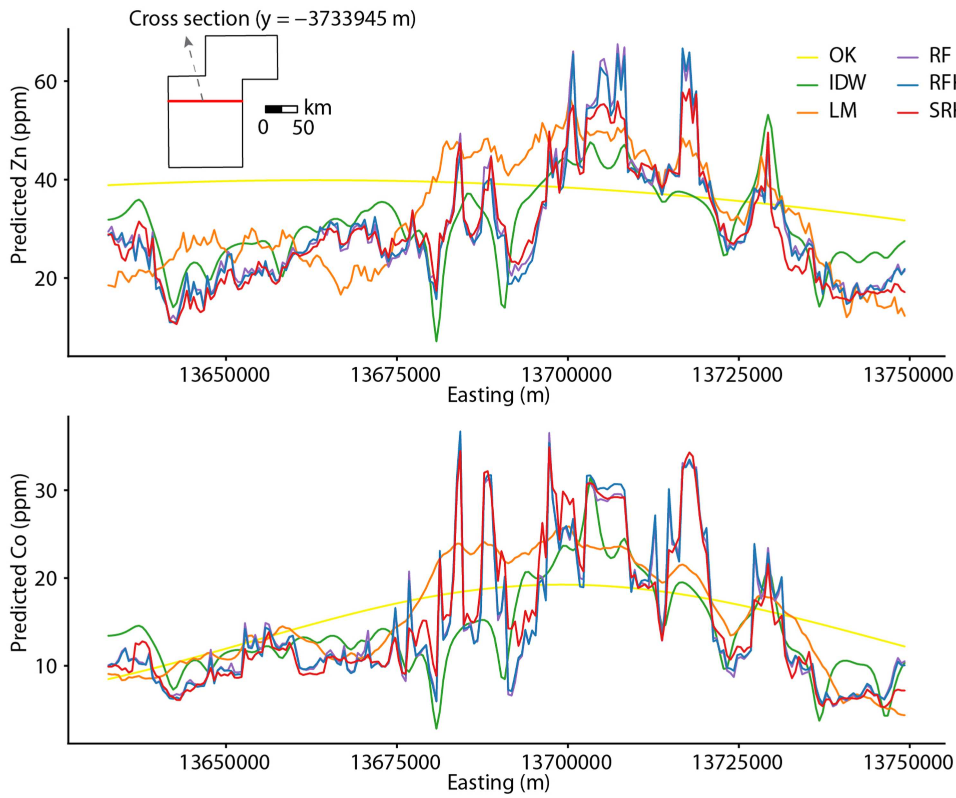

Figure 10. Comparisons of predicted Zn and Co concentrations derived from SRK and benchmark models along a horizontal cross-section at $y = -3733945$ m in the study area.

A horizontal cross-section at $y = -3733945$ m is used in Figure 10 to compare the predicted Zn and Co concentrations among SRK and the benchmark models. Overall, the SRK profiles show clearer local variation than OK and LM, while remaining less fragmented than IDW. RF and RFK capture similar spatial fluctuations, but the SRK curves appear slightly more coherent along the transect. These patterns suggest that SRK provides a more balanced representation of regional continuity and local heterogeneity in cross-section predictions.

Figure 11 compares the prediction uncertainty of RFK and SRK for Zn and Co. For both elements, the uncertainty maps show that SRK produces consistently lower uncertainty than RFK across the study area, which is also reflected in the probability density curves shifting towards smaller values and in the lower mean uncertainty levels of SRK. The difference maps, defined as $\Delta = \delta RFK - \delta SRK$, are uniformly positive, further confirming that SRK yields lower uncertainty than RFK at nearly all prediction locations. These results indicate that SRK produces lower kriging-based prediction uncertainty than RFK under the current modelling framework, although formal calibration of prediction intervals remains an important direction for future evaluation.

5. Discussion

This study introduces the singularity regression kriging (SRK) model as a spatial prediction approach designed to improve trend estimation in environments characterised by nonlinearity and multiscale heterogeneity. Rather than relying solely on the original covariates, SRK augments the random forest trend model with singularity-based covariate features that capture local multiscale contrast and anomaly-related structure. In this way, more spatially structured variation can be absorbed before kriging, potentially producing residuals that are more concentrated and more amenable to ordinary kriging interpolation. By modelling these structures prior to kriging, SRK creates more favourable statistical conditions for geostatistical interpolation.

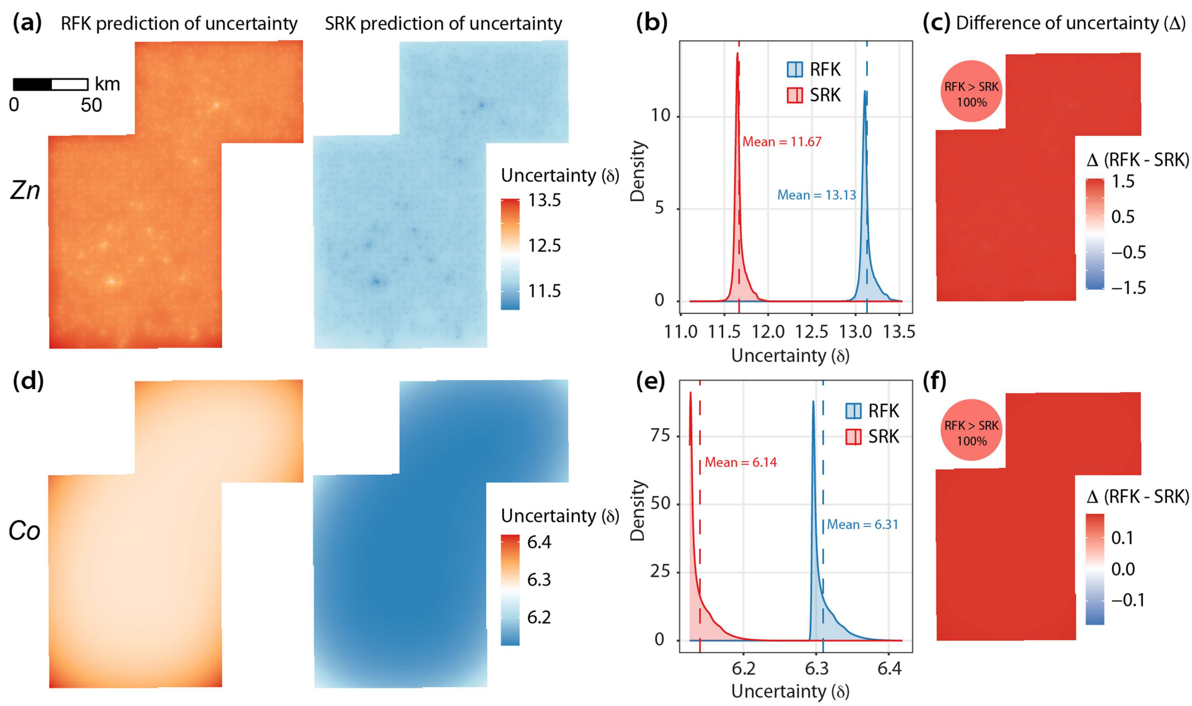

Figure 11. Uncertainty analysis and comparison between the SRK and RFK models for Zn and Co prediction. (a, d) Spatial distributions of prediction uncertainty derived from the RFK and SRK models for Zn and Co, respectively. (b, e) Probability density distributions of uncertainty values for RFK and SRK, with dashed lines indicating mean uncertainty levels. (c, f) Spatial differences in uncertainty, defined as $\Delta = \delta_{RFK} - \delta_{SRK}$, where positive values indicate lower uncertainty for SRK than for RFK.

A key contribution of SRK is the integration of singularity-based anomaly indices into the random forest feature set. These singularity features provide a process-aware description of local heterogeneity that is not readily represented by conventional covariates alone. By incorporating such features into the trend model, SRK enhances the ability of the regression component to capture nonlinear and spatially structured variation in the response field. The simulation experiments further show that the benefits of SRK are most evident under skewed and long-tailed conditions, where conventional kriging assumptions are more likely to be violated. This suggests that SRK is not intended to replace traditional kriging in all settings, but rather to extend its applicability to more complex spatial prediction problems. Thus, SRK is effective when the target variable is affected by nonlinear covariate relationships, multiscale spatial structures, and local anomaly patterns that are not fully represented by the original predictor values. These conditions are common in heterogeneous geological and environmental settings, particularly where the response distribution is skewed, long-tailed, or locally enriched. Under such conditions, covariate singularity features may provide additional information for trend estimation and reduce the amount of structured variation left for residual kriging.

The application to trace element mapping in Western Australia further illustrates the practical value of SRK in heterogeneous geological environments. The residual density comparison in Figure 6 further shows that the residuals from SRK are more concentrated around zero than those from the standard RF model, supporting the role of singularity features in improving the residual structure before kriging. Compared with benchmark methods, SRK produces spatial predictions with more coherent anomaly patterns and smoother transitions while avoiding excessive local oscillations. More importantly, SRK consistently reduces prediction uncertainty across the study area, as evidenced by both spatial uncertainty maps and probability density distributions. This reduction in kriging-based uncertainty suggests that singularity-augmented trend modelling may improve the stability of spatial predictions, although lower uncertainty values should not be interpreted as formal evidence of calibrated prediction intervals.

Despite its advantages, several limitations of SRK should be acknowledged. First, SRK may be less suitable when relevant covariates are unavailable, when covariate singularity features show weak association with the response, or when the study area exhibits limited spatial heterogeneity. In such cases, the singularity features may add little information beyond the original covariates, and simpler methods such as RF, RFK, or conventional kriging may be sufficient. Second, the computation of singularity indices involves multiscale neighbourhood analysis, which increases computational cost relative to RF and RFK, especially for large prediction grids or many covariates. In the present implementation, this additional cost is mainly associated with singularity feature construction, whereas the subsequent random forest fitting and residual kriging follow standard modelling procedures. In addition, model performance can be influenced by the choice of singularity-scale parameters, although these were found to be relatively stable in the present study. Another issue concerns the potential mismatch in support among point samples, environmental covariates, and the 500-m prediction grid. Although this resolution was considered appropriate for the current study area, sampling density, and predictor detail, support effects related to sample clustering and distance-based geological covariates may still influence local prediction behaviour. In addition, although the present study compares SRK with several widely used benchmark methods, further comparisons with alternative non-stationary spatial interpolation approaches, such as filtering-based methods that do not rely on the conventional stationarity assumption, would be a valuable direction for future research. Future research could also explore adaptive or data-driven strategies for parameter selection, evaluate support effects more explicitly across multiple prediction resolutions, extend the approach to spatio-temporal contexts, or investigate alternative anomaly descriptors. Overall, SRK provides a flexible and extensible approach for spatial prediction in complex environments characterised by nonlinearity, multiscale heterogeneity, and anomalous behaviour.

6. Conclusion

This study proposed the singularity regression kriging (SRK) model as a new spatial prediction model that enhances conventional kriging by augmenting trend estimation with covariate singularity features so that nonlinear and multiscale structures are absorbed before kriging. By augmenting the random forest feature set with covariate-based singularity indices and applying ordinary kriging to the resulting residuals, SRK systematically improves the stationarity of residuals prior to kriging. Simulation experiments demonstrated that SRK consistently outperforms ordinary kriging, with particularly pronounced gains under skewed and long-tailed distributions that violate Gaussian assumptions. Application to trace element prediction in a mineralised region of Western Australia further showed, under 5-fold spatial block cross-validation, that SRK produces more coherent spatial patterns, modestly improved predictive performance relative to RF and RFK, and reduced prediction uncertainty. Parameter sensitivity analysis further indicated that the model is robust to moderate changes in singularity-scale settings. These results indicate that explicitly incorporating covariate-based singularity features into trend estimation is important for reliable spatial prediction in heterogeneous geological environments. The SRK model is flexible and extensible, and can be readily applied to other environmental and geoscientific variables characterised by strong nonlinearity, multiscale heterogeneity, and complex spatial dependence.

Author contributions

CRediT: **Kai Ren:** Conceptualization, Data curation, Formal analysis, Methodology, Visualization, Writing – original draft; **Yongze Song:** Conceptualization, Formal analysis, Methodology, Supervision, Visualization, Writing – review & editing; **Min Chen:** Supervision, Writing – review & editing; **Qiang Yu:** Supervision, Writing – review & editing.

Disclosure statement

No potential conflict of interest was reported by the author(s).

Funding

This work was supported by the National Natural Science Foundation of China (Outstanding Young Scholars Programme, Grant No. 42325107) and the Natural Science Foundation of Inner Mongolia Autonomous Region of China (2024QN03070).

ORCID

Kai Ren 0009-0007-1079-902X
Yongze Song 0000-0003-3420-9622
Min Chen 0000-0001-8922-8789
Qiang Yu 0000-0001-6950-1821

Data availability statement

All data used in this study are publicly available. Geochemical data were obtained from the GSWA Geochemistry Database (DMIRS-047) (Department of Energy et al. 2019), lithological data from Geoscience Australia's Surface Geology of Australia dataset (Geoscience Australia 2012), and topographic data from the Geoscience Australia Digital Elevation Model (Geoscience Australia 2015). The data and codes that support the findings of this study are available on Figshare at https://doi.org/10.6084/m9.figshare.31073173 (Ren et al. 2026).

Open scholarship

This article has earned the Centre for Open Science badge for Open Data. The data and materials are openly accessible at (https://doi.org/10.6084/m9.figshare.31073173). To obtain the author's disclosure form, please contact the Editor.

References

Austin, M. P. 2002. "Spatial Prediction of Species Distribution: An Interface between Ecological Theory and Statistical Modelling." *Ecological modelling* 157 (2-3): 101–118. https://doi.org/10.1016/S0304-3800(02)00205-3.

Bao, L.-L., C.-X. Zhang, J.-S. Zhang, and R. Guo. 2024. "A Two-Stage Spatial Prediction Modeling Approach Based on Graph Neural Networks and Neural Processes"." *Expert Systems with Applications* 258: 125173. https://doi.org/10.1016/j.eswa.2024.125173.

Beale, C. M., J. J. Lennon, J. M. Yearsley, M. J. Brewer, and D. A. Elston. 2010. "Regression Analysis of Spatial Data." *Ecology letters* 13(2): 246–264. https://doi.org/10.1111/j.1461-0248.2009.01422.x.

Böhner, J., 2005. Advancements and New Approaches in Climate Spatial Prediction and Environmental Modelling. *Arbeitsberichte des Geographischen Instituts der HU zu Berlin* 109, 49–90.

Böhner, J., and T. Selige. 2006. "Spatial Prediction of Soil Attributes Using Terrain Analysis and Climate Regionalisation." *Gottinger Geographische Abhandlungen* 115: 13–28.

Breiman, L., 2001. Random Forests. *Machine learning* 45 (1), 5–32. https://doi.org/10.1023/A:1010933404324

Chen, L., Chen, Z., Song, Y., Yang, C., He, S., Li, Z., Guo, W., Chen, N., 2026. Spatiotemporal Adaptive Multiscale Transformer for Prediction. *International Journal of Geographical Information Science*, 1–25. https://doi.org/10.1080/13658816.2025.2602536

Cheng, Q., 2012. Singularity Theory and Methods for Mapping Geochemical Anomalies Caused By Buried Sources and for Predicting Undiscovered Mineral Deposits in Covered Areas. *Journal of Geochemical Exploration* 122, 55–70. https://doi.org/10.1016/j.gexplo.2012.07.007

Cheng, Q., 2017. Singularity Analysis of Global Zircon u-pb Age Series and Implication of Continental Crust Evolution. *Gondwana Research* 51, 51–63. https://doi.org/10.1016/j.gr.2017.07.011

Cheng, Q. 2018. "Singularity Analysis of Nonlinear Earth." In *Handbook of Mathematical Geosciences: Fifty Years of IAMG,* 179. https://doi.org/10.1007/978-3-319-78999-6_10

Cressie, N., 1988. Spatial Prediction and Ordinary Kriging. *Mathematical geology* 20 (4), 405–421. https://doi.org/10.1007/BF00892986

Dadashpoor, H., P. Azizi, and M. Moghadasi. 2019. "Analyzing Spatial Patterns, Driving Forces and Predicting Future Growth Scenarios for Supporting Sustainable Urban Growth: Evidence from Tabriz Metropolitan Area, Iran." *Sustainable Cities and Society* 47: 101502. https://doi.org/10.1016/j.scs.2019.101502.

Department of Energy, Mines, Industry Regulation and Safety. 2019. GSWA Geochemistry (DMIRS-047). Accessed: 2025-12-06. URL https://catalogue.data.wa.gov.au/dataset/gswa-geochemistry

Fouedjio, F., and J. Klump. 2019. "Exploring Prediction Uncertainty of Spatial Data in Geostatistical and Machine Learning Approaches." *Environmental Earth Sciences* 78(1): 38. https://doi.org/10.1007/s12665-018-8032-z.

Fouedjio, F., and E. Arya. 2024. "Locally Varying Geostatistical Machine Learning for Spatial Prediction." *Artificial Intelligence in Geosciences* 5: 100081. https://doi.org/10.1016/j.aiig.2024.100081.

Geoscience Australia. 2012. Surface Geology of Australia 1:1 million scale dataset (2012 edition). https://data.gov.au/data/dataset/surface-geology-of-australia-1-1-million-scale-dataset-2012-edition

Geoscience Australia. 2015. Digital Elevation Model (DEM) of Australia derived from LiDAR 5 Metre Grid. Geospatial dataset.

Hengl, T., G. B. Heuvelink, and A. Stein. 2004. "A Generic Framework for Spatial Prediction of Soil Variables Based on Regression-Kriging." *Geoderma* 120(1-2): 75–93. https://doi.org/10.1016/j.geoderma.2003.08.018.

Hengl, T., G. B. Heuvelink, and D. G. Rossiter. 2007. "About Regression-Kriging: From Equations to Case Studies." *Computers & geosciences* 33(10): 1301–1315. https://doi.org/10.1016/j.cageo.2007.05.001.

Hengl, T., M. Nussbaum, M. N. Wright, G. B. Heuvelink, and B. Gräler. 2018. "Random Forest as a Generic Framework for Predictive Modeling of Spatial and Spatio-Temporal Variables." *PeerJ* 6: e5518. https://doi.org/10.7717/peerj.5518.

Holdaway, M. R., 1996. Spatial Modeling and Interpolation of Monthly Temperature Using Kriging. *Climate research* 6, 215–225. https://doi.org/10.3354/cr006215

Isaaks, E., and R. M. Srivastava. 1988. "Spatial Continuity Measures for Probabilistic and Deterministic Geostatistics." *Mathematical geology* 20(4): 313–341. https://doi.org/10.1007/BF00892982.

Janssen, S., G. Dumont, F. Fierens, and C. Mensink. 2008. "Spatial Interpolation of Air Pollution Measurements Using Corine Land Cover Data." *Atmospheric Environment* 42(20): 4884–4903. https://doi.org/10.1016/j.atmosenv.2008.02.043.

Jerrett, M., S. Gale, and C. Kontgis. 2010. "Spatial Modeling in Environmental and Public Health Research." *International journal of environmental research and public health* 7(4): 1302–1329. https://doi.org/10.3390/ijerph7041302.

Jones, P. G., and P. K. Thornton. 2002. "Spatial Modeling of Risk in Natural Resource Management." *Conservation ecology* 5(2). https://doi.org/10.5751/ES-00324-050227.

Kingsley, J., S. O. Lawani, A. O. Esther, K. M. Ndiye, O. J. Sunday, and V. Penížek. 2019. "Predictive Mapping of Soil Properties for Precision Agriculture Using Geographic Information System (Gis) Based Geostatistics Models." *Modern Applied Science* 13(10): 60–77. https://doi.org/10.5539/mas.v13n10p60.

Kupfer, J. A., and C. A. Farris. 2007. "Incorporating Spatial Non-Stationarity of Regression Coefficients into Predictive Vegetation Models." *Landscape Ecology* 22(6): 837–852. https://doi.org/10.1007/s10980-006-9058-2.

Li, J., 2016. Assessing Spatial Predictive Models in the Environmental Sciences: Accuracy Measures, Data Variation and Variance Explained. *Environmental Modelling & Software* 80, 1–8. https://doi.org/10.1016/j.envsoft.2016.02.004

Li, X., Y. Ao, S. Guo, and L. Zhu. 2019. "Combining Regression Kriging with Machine Learning Mapping for Spatial Variable Estimation." *IEEE Geoscience and Remote Sensing Letters* 17(1): 27–31. https://doi.org/10.1109/LGRS.2019.2914934.

Liu, X., J. Wu, and J. Xu. 2006. "Characterizing the Risk Assessment of Heavy Metals and Sampling Uncertainty Analysis in Paddy Field By Geostatistics and Gis." *Environmental pollution* 141(2): 257–264. https://doi.org/10.1016/j.envpol.2005.08.048.

Liu, X., O. Kounadi, and R. Zurita-Milla. 2022. "Incorporating Spatial Autocorrelation in Machine Learning Models Using Spatial Lag and Eigenvector Spatial Filtering Features." *ISPRS International Journal of Geo-Information* 11(4): 242. https://doi.org/10.3390/ijgi11040242.

Luo, P., Y. Wu, and Y. Song. 2026b. "Focal-Feature Regression Kriging." *Geographical Analysis* 58(2): e70035. https://doi.org/10.1111/gean.70035.

Luo, P., Y. Li, Y. Song, Z. Li, and L. Meng. 2026a. "Measuring Univariate Effects in the Interaction of Geographical Patterns." *International Journal of Geographical Information Science* 40(2): 382–413. https://doi.org/10.1080/13658816.2025.2526042.

Meyer, H., Pebesma, E., 2021. Predicting into Unknown Space? Estimating the Area of Applicability of Spatial Prediction Models. *Methods in Ecology and Evolution* 12 (9), 1620–1633. https://doi.org/10.1111/2041-210X.13650

Milne, B. T., 1991. Heterogeneity as a Multiscale Characteristic of Landscapes. In: Ecological heterogeneity. Springer, pp. 69–84. 86 *Ecological Studies* https://doi.org/10.1007/978-1-4612-3062-5_4

Odeh, I. O., A. McBratney, and D. Chittleborough. 1995. "Further Results on Prediction of Soil Properties from Terrain Attributes: Heterotopic Cokriging and Regression-Kriging." *Geoderma* 67(3-4): 215–226. https://doi.org/10.1016/0016-7061(95)00007-B.

Oliver, M. A., and R. Webster. 1990. "Kriging: A Method of Interpolation for Geographical Information Systems." *International Journal of Geographical Information System* 4(3): 313–332. https://doi.org/10.1080/02693799008941549.

Papritz, A. and A. Stein. 1999. *Spatial prediction by linear kriging. In: Spatial statistics 637 for remote sensing*83–113.Springer, .

Raymond, O. L., S. Liu, R. Gallagher, W. Zhang, and L. M. Highet. 2012. Surface geology of australia 1:1 million scale dataset. 2012https://dx.doi.org/10.26186/74619

Ren, K., Y. Song, M. Chen, and Q. Yu. 2026. *Code and data for singularity regression kriging (srk) model*, https://doi.org/10.6084/m9.figshare.31073173.

Ren, K., Y. Song, L. Li, F. Mancini, Z. Xiao, X. Zhang, R. Qu, and Q. Yu. 2025. "Identifying Climate and Environmental Determinants of Spatial Disparities in Wheat Production Using a Geospatial Machine Learning Model." *GIScience & Remote Sensing* 62(1): 2533487. https://doi.org/10.1080/15481603.2025.2533487.

Sekulić, A., Kilibarda, M., Heuvelink, G. B., Nikolić, M., Bajat, B., 2020. Random Forest Spatial Interpolation. *Remote Sensing* 12 (10), 1687. https://doi.org/10.3390/rs12101687

Selby, B., and K. M. Kockelman. 2013. "Spatial Prediction of Traffic Levels in Unmeasured Locations: Applications of Universal Kriging and Geographically Weighted Regression." *Journal of Transport Geography* 29: 24–32. https://doi.org/10.1016/j.jtrangeo.2012.12.009.

Sen, Z., 2016. *Spatial modeling principles in earth sciences*. Springer.

Song, Y., 2022. The Second Dimension of Spatial Association. *International Journal of Applied Earth Observation and Geoinformation* 111, 102834. https://doi.org/10.1016/j.jag.2022.102834

Song, Y., 2023. Geographically Optimal Similarity. *Mathematical Geosciences* 55 (3), 295–320. https://doi.org/10.1007/s11004-022-10036-8

Song, Y., P. Wu, Q. Li, Y. Liu, and L. Karunaratne. 2021. “Hybrid Nonlinear and Machine Learning Methods for Analyzing Factors Influencing the Performance of Large-Scale Transport Infrastructure.” *IEEE Transactions on Intelligent Transportation Systems* 23(8): 12287–12300. https://doi.org/10.1109/TITS.2021.3112458.

Sparrow, B. D., W. Edwards, S. E. Munroe, G. M. Wardle, G. R. Guerin, J.-F. Bastin, B. Morris, R. Christensen, S. Phinn, and A. J. Lowe. 2020. “Effective Ecosystem Monitoring Requires a Multi-Scaled Approach.” *Biological reviews* 95(6): 1706–1719. https://doi.org/10.1111/brv.12636.

Talebi, H., Peeters, L. J., Otto, A., Tolosana-Delgado, R., 2022. A Truly Spatial Random Forests Algorithm for Geoscience Data Analysis and Modelling. *Mathematical Geosciences* 54 (1), 1–22. https://doi.org/10.1007/s11004-021-09946-w

Vann, J., and D. Guibal. 1998. “Beyond Ordinary kriging–an Overview of Non-Linear Estimation.” *In: Proceedings of a one day symposium: Beyond Ordinary Kriging* Vol. 32: 6–25.

Waller, L. A. and C. A. Gotway. 2004. Applied Spatial Statistics for Public Health Data John Wiley & Sons.

Wu, T., and Y. Li. 2013. “Spatial Interpolation of Temperature in the United States Using Residual Kriging.” *Applied Geography* 44: 112–120. https://doi.org/10.1016/j.apgeog.2013.07.012.

Xu, D., X. Peng, Q. Tang, and Y. Song. 2025. “Urbanization’S Role in Shaping Ornamental Tree Diversity: A Remote Sensing and Future Scenario-Based Perspective.” *GIScience & Remote Sensing* 62(1): 2557050. https://doi.org/10.1080/15481603.2025.2557050.

Yang, J., Q. Liu, X. Mao, Z. Liu, Y. Zhu, and M. Deng. 2024. “Generalized Yang Chizhong Filtering and Interpolation Method Without Stationarity Assumption.” *International Journal of Geographical Information Science* 38(7): 1360–1387. https://doi.org/10.1080/13658816.2024.2344186.

Yang, X., Y. Song, C. Yoo, K. Ren, and P. Wu. 2025. “Irregular Anisotropy in Surface Urban Heat Island Footprint.” *Sustainable Cities and Society* 131: 106779. https://doi.org/10.1016/j.scs.2025.106779.